ML-Physical Fusion Models Are Accelerating the Paradigm Shift in Operational Typhoon Forecasting

Zeyi Niu[1,2*]

[1]Shanghai Typhoon Institute, and Key Laboratory of Numerical Modeling for Tropical Cyclone of the China Meteorological Administration, Shanghai, China.
[2]Department of Atmospheric and Oceanic Sciences and Institute of Atmospheric Sciences, Fudan University, Shanghai 200438, China.

Key Points:

- This study combines the FuXi model and the Shanghai Typhoon Model to create a hybird operational typhoon forecasting paradigm.
- Using the strengths of both models, FuXi-SHTM improves the accuracy of typhoon track, intensity, and precipitation prediction.
- Proposed a novel workflow of assimilating target observation in CNOP-sensitive area of FuXi-SHTM hybrid model.

Corresponding author: Zeyi Niu, `niuzy@typhoon.org.cn`

Abstract

In this study, we develop a hybrid operational typhoon forecasting model that integrates the FuXi machine-learning (ML) model with the physics-based Shanghai Typhoon Model (SHTM) into a dual physics–data-driven framework. By employing spectral nudging, the hybrid model named FuXi-SHTM leverages FuXi's robust large-scale forecasting capabilities alongside SHTM's mesoscale strengths, significantly enhancing track, intensity, and precipitation predictions for super typhoons Yagi (2024) and Krathon (2024). Besides, this study aims to identify the sensitive regions for the hybrid model by using Conditional Nonlinear Optimal Perturbation (CNOP) method. Despite being constrained by FuXi's large-scale forecast fields, the dense assimilation of satellite observations within these sensitive regions can further enhance typhoon forecasts. Besides, this study offers key insights into the emerging paradigms that are set to shape the future development of both machine learning and physics-based modeling approaches.

Plain Language Summary

Accurate typhoon forecasting is crucial for effective disaster preparedness. In this study, we developed a hybrid model that integrates the machine-learning-based FuXi model with the physics-based Shanghai Typhoon Model (SHTM) using spectral nudging. This approach leverages FuXi's strength in capturing large-scale weather patterns and SHTM's ability to resolve finer mesoscale details, thereby improving predictions of a typhoon's track, intensity, and rainfall. Additionally, we identified key observation-sensitive regions using the Conditional Nonlinear Optimal Perturbation (CNOP) method and found that assimilating satellite data from these regions further improved the forecasts. Overall, our findings highlight the potential of integrating machine learning with physical models to advance operational typhoon predictions.

1 Introduction

With the rapid development of data-driven machine-learning (ML) models such as PanGu, GraphCast, FuXi, and ECMWF AIFS (Bi et al., 2023; Lam et al., 2023; Chen et al., 2023; Lang et al., 2024), these models have demonstrated a clear advantage over traditional global/regional numerical weather prediction (NWP) systems in reducing tropical cyclone track forecast errors (Ben-Bouallegue et al., 2023; C. C. Liu et al., 2024). However, significant shortcomings remain in the forecasting of the intensity of the cyclone. This is mainly because these ML models are trained on the ERA5 reanalysis dataset, which is limited by its horizontal resolution and further hampered by the 'double penalty' effect in the loss function (Bonavita et al., 2024; Subich et al., 2025). Consequently, models do not adequately resolve mesoscale features, leading to a systematic underestimate of the intensity of tropical cyclones (Sun et al., 2024; Xu et al., 2025). Moreover, these large ML models suffer from weak physical interpretability and cannot provide a comprehensive set of forecast variables to represent the current weather state, which poses significant limitations (Husain et al., 2024). Therefore, enhancing the contribution of ML models in forecasting high-impact weather remains a current research hotspot (Olivetti and Messori, 2024).

Recent studies indicate that incorporating physical constraints into ML models can improve forecast performance. For example, Zhang et al. (2023) developed the NowcastNet model for short-term precipitation forecasting by integrating the water vapor transport equation within a neural network framework and optimizing it end-to-end, thereby enhancing forecast accuracy. Similarly, NeuralGCM incorporates physical parameterization schemes into its neural network architecture to ensure that forecast outputs adhere to fundamental atmospheric principles, thus improving both forecast efficiency and performance (Kochkov et al., 2024). Alternatively, hybrid models that incorporate constraints from ML models into traditional physics-based systems also show promise in improving high-resolution tropical cyclone forecasts. For instance, Xu et al. (2024) improved extreme precipitation forecasts

by driving a regional high-resolution Weather Research and Forecasting (WRF) model with the PanGu model, while Liu et al. (2024) enhanced tropical cyclone track and intensity predictions by integrating the PanGu model with a regional coupled ocean-atmosphere model. The Canadian Environment and Climate Change Department (ECCC) also achieved significant forecast improvements by merging the Global Environmental Multiscale (GEM) and GraphCast models (Husain et al., 2024).

Although the machine-learning and physics-based hybrid model indicates that a new paradigm for operational tropical cyclone forecasting is gradually maturing, the associated operational workflows for this hybrid system remain underdeveloped. It is still unclear whether data assimilation can be employed to reduce the forecast errors of the hybrid model, and what the spatial scale of such error reductions might be (Niu et al., 2025). Moreover, an integrated operational workflow for target observation–assimilation forecasting for the hybrid model has not yet been established. Therefore, this study is the first to use Conditional Nonlinear Optimal Perturbation (CNOP) (Mu et al., 2003) method to calculate the target sensitive areas of the hybrid model and to improve typhoon forecasts by densifying the assimilation of satellite data within these sensitive regions. This study will provide valuable guidance for the future refinement of the operational paradigm of the machine-learning and physics-based hybrid model.

2 Model and Methods

2.1 ECMWF HRES, FuXi, and SHTM

ECMWF High Resolution Forecast System (HRES) is currently recognized as one of the best-performing global NWP systems, with a horizontal resolution of 9 km and 137 vertical model levels. The Shanghai Meteorological Service currently receives the HRES D1D product in real time. Its upper-level variables are provided at a horizontal resolution of 0.2°×0.2° across 19 pressure levels (10, 20, 70, 100, 150, 200, 250, 300, 400, 500, 600, 700, 800, 850, 900, 925, 950, and 1000 hPa), while its surface variables have a horizontal resolution of 0.1°×0.1°. The HRES D1D product supplies real-time initial fields for the operational FuXi and SHTM systems.

The FuXi model architecture consists of three primary components: cube embedding, a U-Transformer, and fully connected layers. It is trained and evaluated on 39 years of ERA5 reanalysis data. Evaluations indicate that FuXi performs comparably to the ECMWF ensemble mean and extends the effective forecast lead time, defined as the period during which the anomaly correlation coefficient (ACC) exceeds 0.6, to 10.5 days for 500-hPa geopotential height (Z500). Furthermore, FuXi demonstrates a significant advantage over other machine learning models in forecasting typhoon tracks (Chen et al., 2023). The FuXi model operates at a horizontal resolution of 0.25°×0.25° and produces forecast variables on 13 pressure levels (50, 100, 150, 200, 250, 300, 400, 500, 600, 700, 850, 925, and 1000 hPa). Its upper-level outputs include geopotential height, temperature, specific humidity, and the u- and v-components of wind, while the surface variables comprise surface temperature, mean sea level pressure, 2-m temperature, 10-m wind components, and precipitation.

The operational Shanghai Typhoon Model is based on WRF version 4.0 and is initialized twice daily at 0000 and 1200 UTC to produce forecasts for the following 120 hours. The model domain, comprising 953×701 grid points at a 9-km resolution, spans from 0.5°S to 61.5°N and from 58.3°E to 172.7°E (black domain in Fig. 1a). For consistency with FuXi, the model top is set at 50 hPa in this study. Since 2024, SHTM has employed ECMWF HRES rather than NCEP GFS for its initial and boundary conditions. Moreover, SHTM utilizes the Thompson microphysics scheme (Thompson et al., 2004), the multi-scale Kain–Fritsch cumulus scheme (Budakoti et al., 2019), the rapid radiative transfer model for both longwave and shortwave radiation (Mlawer et al., 1997), the unified Noah land-surface model (Ek et al., 2003), and the Yonsei University planetary boundary layer scheme (Hu et al., 2013).
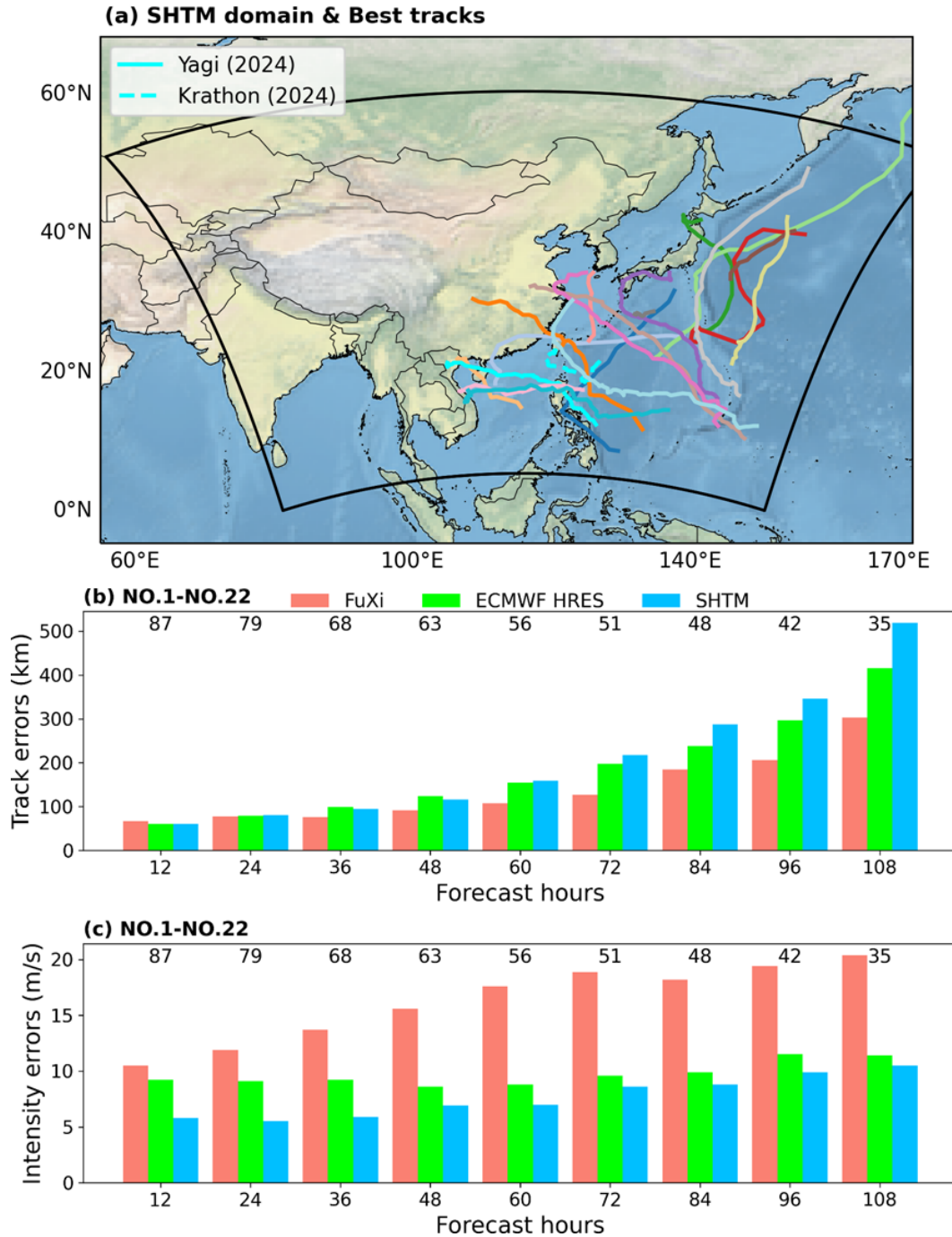
(a) SHTM domain & Best tracks

Figure 1. (a) Best tracks for Northwest Pacific typhoons numbered 202401 to 202422 in 2024. The black curves stand for the SHTM domain (9-km). (b)-(c) Mean track errors and maximum sustained wind errors of selected 22 typhoons along with the different forecast hours from FuXi (light red), ECMWF HRES (light green), and SHTM (light blue), respectively. The numbers in black stand for the sample sizes of different forecast hours.

This study also compares the track and intensity forecasts of 22 typhoons in the Northwest Pacific in 2024 produced by the FuXi, ECMWF HRES, and SHTM models. Figure 1a displays the best tracks for the 22 typhoons numbered 202401 to 202422 as provided by the Regional Specialized Meteorological Center (RSMC) in Tokyo. Landfalling typhoons, such as Typhoon Yagi and Typhoon Krathon, generally exhibit more extreme characteristics, present greater forecasting challenges, and affect broader regions, thereby imposing higher performance requirements on forecast models. Consequently, it is essential for a model to not only accurately predict the track and intensity but also precisely represent the wind and precipitation structures of typhoons. With respect to typhoon track forecasts (Fig. 1b), FuXi performs best, followed by HRES, while SHTM lags slightly behind. Specifically, FuXi achieves an average track error of approximately 100 km at 72 hours—a level of accuracy that is highly commendable. Although SHTM performs comparably to HRES for lead times up to 72 hours, its performance deteriorates at longer lead times. In terms of typhoon intensity forecasts (Fig. 1c), FuXi exhibits the largest intensity errors, whereas the mesoscale SHTM retains an advantage in predicting typhoon intensity. Therefore, a key focus of this study is to integrate FuXi's superior track forecasting capability with SHTM's strength in intensity prediction to achieve optimal overall typhoon forecasts.

2.2 Spectral Nudging

To combine the large-scale forecast fields from FuXi with those from SHTM, this study adopts the traditional spectral nudging (SN) approach. The main equation is given as follows:

$$F_{\text{nudge}} = F_{\text{SHTM}} + \omega[F_{\text{FuXi}} - F_{\text{SHTM}}]_{LS} \qquad (1)$$

where F_{SHTM} denotes the prognostic variable forecast by SHTM dynamics, and F_{FuXi} represents the corresponding FuXi prediction at the same valid time. The parameter ω, which ranges between 0 and 1, serves as the nudging relaxation factor, and F_{nudge} is the resulting nudged solution. The subscript LS indicates the large-scale features targeted by the nudging process. As seen in the equation, the large-scale component in F_{nudge} is a weighted average of F_{SHTM} and F_{FuXi}, with ω as the weighting factor, while the small-scale features from F_{SHTM} are retained in F_{nudge}.

Besides, the parameters are optimized for SN as follows: (i) for the nudged variables, we only used the u- and v-components of wind and virtual temperature, excluding specific humidity, as its inclusion would weaken the intensity forecasts for tropical cyclones (Husain et al., 2024); (ii) the nudging vertical profile was configured to exclude nudging in the boundary layer (below 850 hPa), as the 13-level FuXi model does not offer sufficient vertical resolution at the boundary layer to provide an effective reference; (iii) for the nudging length scales, we selected the Rossby radius (around 1000 km) as the cutoff wavelength for spectral nudging, meaning that scales larger than 1000 km in FuXi are fully retained, while smaller scales are eliminated; (vi) the nudging relaxation time, tau, analogous to the e-folding time, governs the rate at which large-scale differences between the model and driving data decay in the absence of other processes. Given that FuXi's forecasts have a 6-hour interval, we set tau to 6 hours to avoid interpolation errors (Omrani et al., 2012); (v) additionally, since FuXi does not provide sea surface temperature (SST) forecasts, we initialized the SST field using the ECMWF HRES SST data, as the absence of SST data typically results in significant underestimation of typhoon intensity.

2.3 CNOP

The CNOP technique is designed to calculate the initial errors that exert the greatest impact on the forecast field in a verification area. Its primary objective is to determine

an optimal initial perturbation, denoted as δX_0^*, which maximizes a specified cost function under the constraint of

$$\delta X_0^T C_0 \delta X_0 \leq \beta. \tag{2}$$

$$J(\delta X_0^*) = \max_{\delta X_0^T C_0 \delta X_0 \leq \beta} J(\delta X_0), \tag{3}$$

where $J(\delta X_0)$ is defined as:

$$J(\delta X_0) = \left[\boldsymbol{M}(X_0 + \delta X_0) - \boldsymbol{M}(X_0) \right]^T C_t \left[\boldsymbol{M}(X_0 + \delta X_0) - \boldsymbol{M}(X_0) \right] = \delta X_t^T C_t \delta X_t. \tag{4}$$

X_0 is the initial state vector of the model, $\boldsymbol{M}$ is a non-linear forecast model which is FuXi-SHTM in this study. $\boldsymbol{M}(X_0 + \delta X_0) - \boldsymbol{M}(X_0) = \delta X_t$ represents the non-linear evolution of perturbation δX_0. The subscripts 0 and t indicate the initial and verification times. Positive definite matrices C_1 and C_2 serve as the metrics for the initial perturbation δX_0 and its subsequent nonlinear evolution, respectively. In this study, where C is total dry energy in a continuous expression:

$$\delta X^T C \delta X = \int_D \int_0^1 \left[u'^2 + v'^2 + \frac{C_p}{T_r} T'^2 + \frac{(L_v q_v')^2}{C_p T_r} \right] d\sigma dD. \tag{5}$$

Here, D denotes the whole domain region for C_0, and the verification region for C_t, respectively, and σ represents the vertical coordinate. The specific heat capacity at constant pressure is set as $C_p = 1005.7$ J kg^{-1} K^{-1}, and the latent heat of vaporization is $L_v = 2.501 \times 10^6$ J kg^{-1}. The parameter T_r is fixed at 270 K. The perturbation fields u', v', T', and q_v' denote the zonal wind, meridional wind, temperature, and water vapor mixing ratio, respectively. More details can be found in Wang et al. (2011). Notably, the tangent linear and adjoint model (i.e., WRFPLUS) of the SHTM is employed to compute the optimal perturbation. In this study, however, FuXi's forecast field is only used as external forcing to weakly constrain the SHTM forecast. FuXi's tangent linear and adjoint models are not utilized to solve for δX_0^* during the optimization period, primarily because we do not have access to FuXi's source code—a limitation that requires further investigation.

3 Results

The forecast performance of the hybrid model FuXi-SHTM is examined using two super typhoons, Typhoon Yagi (2024) and Typhoon Krathon (2024). Figure 2 shows the best tracks and maximum wind speeds for these two typhoons, along with 0–120 hour forecasts from SHTM and FuXi-SHTM, initialized at 0000 UTC on 3 September 2024 and 1200 UTC on 29 September 2024, respectively. It is evident that SHTM's forecast track for Typhoon Yagi is biased too far to the north, whereas FuXi-SHTM produces a track that is shifted further south and aligns closely with the observations (Fig. 2a). In terms of intensity, FuXi-SHTM performs comparably to SHTM for Typhoon Yagi, though it tends to slightly underestimate the peak intensity (Fig. 2c). Beyond 72 hours, as FuXi-SHTM continues to simulate the typhoon over the ocean while SHTM depicts landfall and subsequent decay, FuXi-SHTM yields a more accurate intensity forecast. Moreover, the intensity forecasts from the standalone FuXi model fall notably short of the observed values. For Typhoon Krathon, FuXi-SHTM not only matches the observed track during the first 66 hours but also maintains a slower movement after 66 hours compared to SHTM (Fig. 2b). Although both SHTM and FuXi-SHTM tend to underestimate the intensity relative to observations,

they still outperform the FuXi forecast in this regard (Fig. 2d). Overall, owing to FuXi's accurate large-scale field, the hybrid FuXi-SHTM model shows marked improvements in typhoon track forecasts over SHTM. Figs.2e-f present the domain-averaged kinetic energy spectra of 66 hour forecasted winds from SHTM and FuXi-SHTM for the two initialization times, along with the energy spectra at individual model levels. It is clear that the energy spectra of FuXi-SHTM and SHTM differ significantly at large scales (greater than 1000 km), while they are essentially similar at mesoscale and smaller scales. This discrepancy arises from the inclusion of FuXi's large-scale forecast field in the FuXi-SHTM model.

In this study, typhoon precipitations are also evaluated for both FuXi-SHTM and SHTM. Figure 3 displays the 24 hour accumulated precipitation from SHTM, FuXi-SHTM, and Automatic Weather Station (AWS) observations over the periods of 48–72, 72–96, and 96–120 hours, with an initial forecast time of 0000 UTC on 3 September 2024. The corresponding Threat Score (TS) values for 24 hour accumulated precipitation for both models (Fig. 3j-l). The TS scores indicate that FuXi-SHTM exhibits a clear advantage across various precipitation thresholds, particularly showing substantial improvements for heavy rainfall (exceeding 100 mm) and extreme rainfall (exceeding 250 mm) during the 96–120 hour period. In terms of precipitation distribution, FuXi-SHTM produces a broader outer rainband for the typhoon (Figs. 3b and 3e), with precipitation over Guangdong (GD) and Hainan (HN) provinces aligning more closely with observations. In contrast, SHTM generates a more compact typhoon structure (Figs. 3a and 3d), resulting in significant underprediction of precipitation in these regions—a discrepancy that is partially attributable to track errors. Furthermore, for the strong rainfall observed in southwestern Guangxi (GX) province following landfall, FuXi-SHTM (Fig. 3h) captures both the location and intensity of the rainfall in agreement with observations, particularly in the extreme rainfall areas (exceeding 250 mm, depicted in deep red) as confirmed by AWS observations (Fig. 3i).

To further enhance the forecasting performance of the FuXi-SHTM hybrid model, this study develops an integrated workflow for target observation-assimilation-forecasting using the CNOP method. For practical use, the CNOP method (Section 2.3) is applied to the FuXi-SHTM model with a 27-km resolution to find the optimal initial perturbations. Since the optimization objective is the 48-hour forecast of Typhoon Yagi, the verification region is selected as a 4-degree latitude-longitude box centered on the position of Typhoon Yagi after 48 hours (magenta box in Fig. 4a). The total dry energy of the CNOP is calculated for each model grid point and integrated in the vertical direction. They are then ranked, with the top 5%-10% defined as the level 1 sensitive area, the top 2.5%-5% as level 2, and the top 2.5% as level 3. The higher the level, the greater the impact of the initial perturbations in this area on the forecast in the verification area. Fig. 4b shows the CNOP-based temperature perturbations for the 25th layer (around 425 hPa) and the 30th layer (around 293 hPa) of the model. It can be observed that the perturbation distribution exhibits a clear alternating positive-negative structure. Minimizing the initial errors of this distribution is expected to have the greatest improvement in the typhoon forecast.Therefore, this study investigates the assimilation of Fengyun (FY)-4B Advanced Geosynchronous Radiation Imager (AGRI) observations for the CNOP-sensitive area of the hybrid model. The assimilation system used is Gridpoint Statistical Interpolation (GSI) version 3.7, and the three-dimensional variational data assimilation (3DVAR) method was employed to assimilate the FY-4B clear-sky brightness temperatures from the water vapor channels 9-11, and window channel 13 (around 10.7 μm). The details of assimilations of FY-4B AGRI in GSI3.7 can be in Niu et al. (2024). To highlight the assimilation effects within the CNOP-sensitive area and to compare the impact of assimilation with and without enhanced assimilation in this area, three assimilation experiments were designed: DAEXP_all, DAEXP_inCNOP120, and DAEXP_inCNOP30. These represent assimilation of all FY-4B AGRI clear-sky observations with a 120 km thinning grid, assimilation only of FY-4B AGRI clear-sky observations in the CNOP-sensitive area with a 120 km thinning grid, and assimilation only of FY-4B AGRI clear-sky observations in the CNOP-sensitive area with a 30 km thinning grid, respectively. Fig. 4c-d show the spatial distributions of
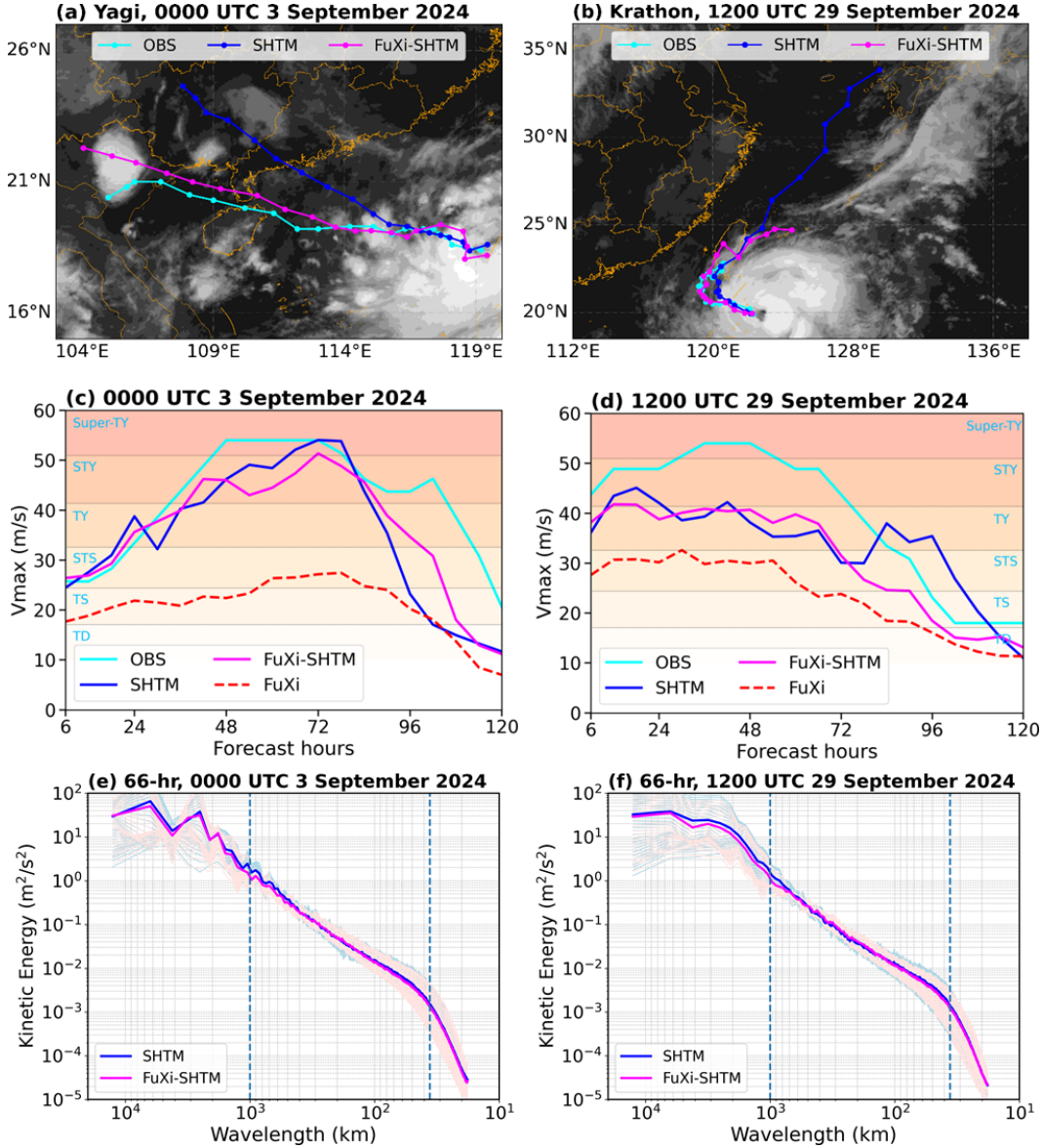
Figure 2. (a)-(b) Best tracks and (c)–(d) maximum wind speed ($V_{\max}$, unit: m s^{-1}) for Typhoon Yagi (2024) and Typhoon Krathon (2024), along with 6–120 hr forecasts from SHTM (blue) and FuXi-SHTM (magenta) initialized at 0000 UTC 3 September 2024 and 1200 UTC 29 September 2024, respectively. The FuXi forecast track is almost the same as the FuXi-SHTM, so it is not shown.(e)-(f) Domain-averaged kinetic energy spectra of 66-hr forecasted winds from SHTM (blue) and FuXi-SHTM (magenta) for the two different initialization times. The kinetic energy spectra for each model level from SHTM (light blue) and FuXi-SHTM (light pink) are shown. The vertical dashed lines stand for 100 km and 36 km, respectively.
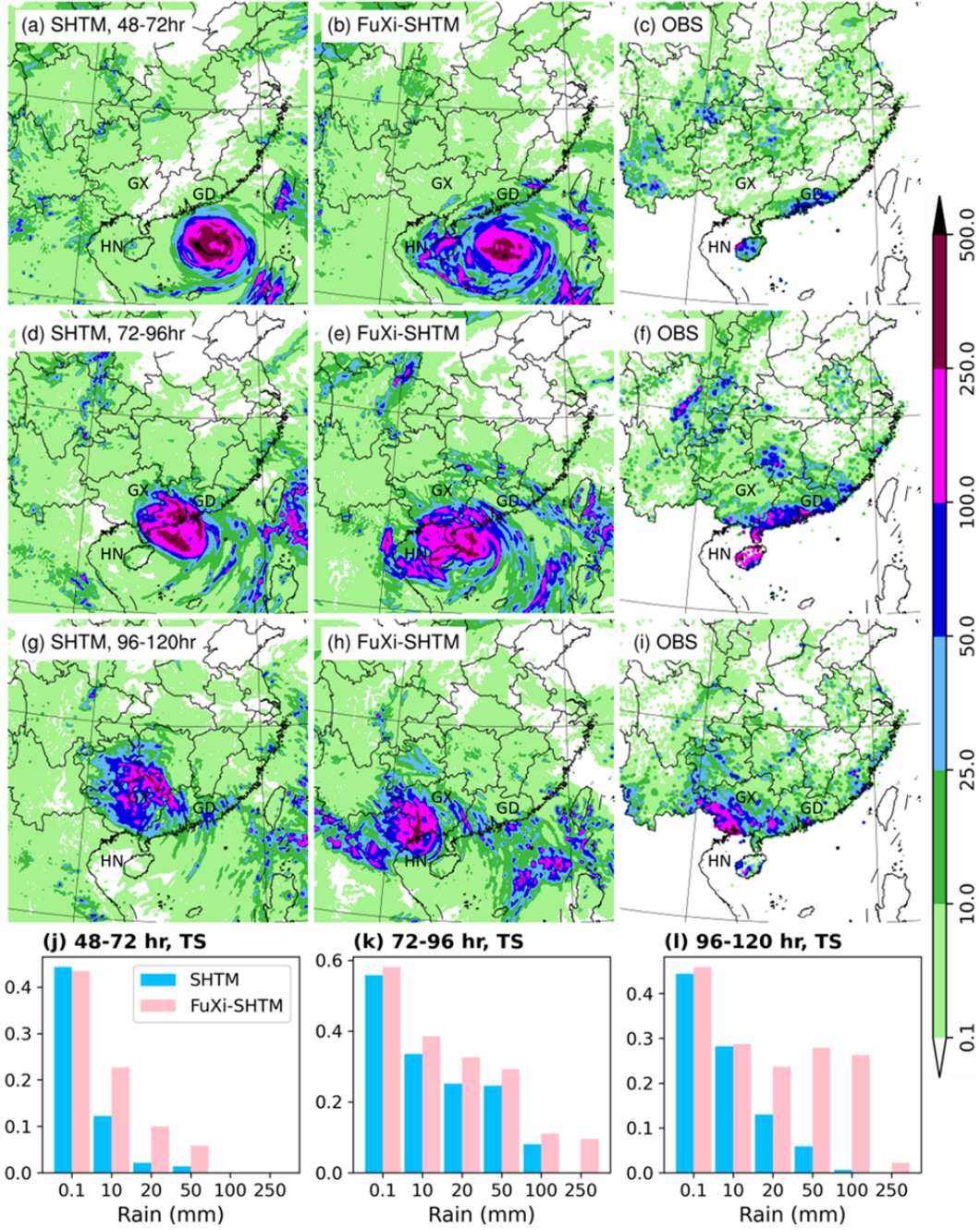
Figure 3. 24-hour accumulated precipitation (unit: mm) of SHTM (left), FuXi-SHTM (middle), and Automatic Weather Station (AWS) observations (right) over the periods of (a)–(c) 48–72 hours, (d)–(f) 72–96 hours, and (g)–(i) 96–120 hours with the initial forecasting time at 0000 UTC 3 September 2024. Threat score (TS) values of 24-hour accumulated precipitation over the periods of (j) 48–72 hours, (k) 72–96 h, and (l) 96–120 h for the SHTM (light blue) and FuXi-SHTM (light pink).
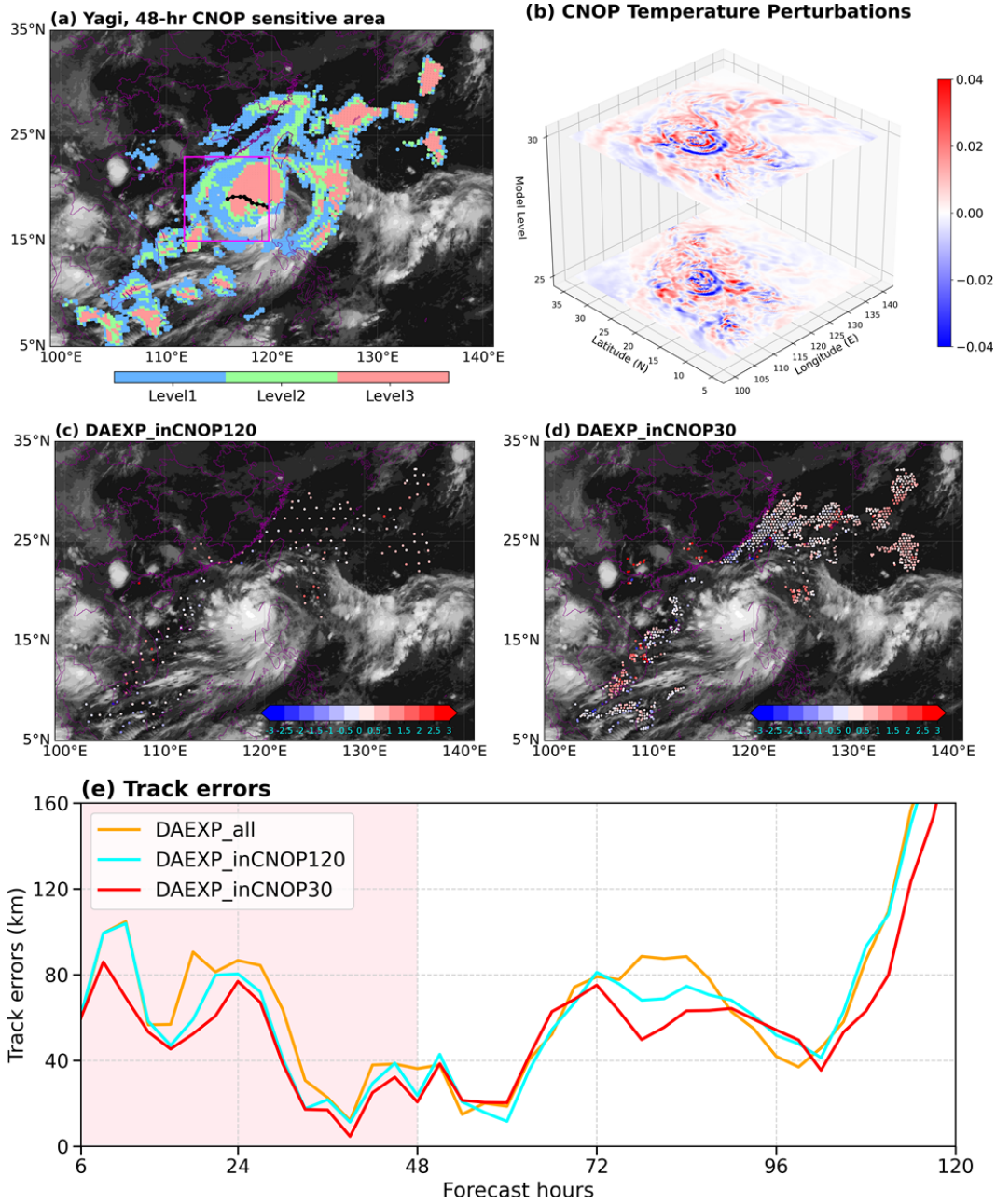
Figure 4. (a) The sensitive areas (shaded; levels 1-3) calculated by CNOP in the rectangle (magenta box, validation area) over 48 optimization period for case Yagi (2024) with the initial time at 0000 UTC 3 September 2024. The black dots stand for the best track from 0000 UTC 3 September 2024 to 0000 UTC 5 September 2024. (b) Spatial distribution of the initial temperature perturbations (unit: K) at model levels 25 and 30 calculated from CNOP method. (c)-(d) Spatial distributions of O–B values of the clear-sky FY-4B AGRI channel-9 in CNOP area with 120-km (DAEXP_inCNOP120) and 30-km (DAEXP_inCNOP30) thinning box, respectively. The background stands for the FY-4B AGRI channel-13 brightness temperatures. (e) Forecasted track errors of experiments DAEXP_all (yellow), DAEXP_inCNOP120 (cyan), and DAEXP_inCNOP30 (red), respectively, for typhoon Yagi (2024) with the initial time at 0000 UTC 3 September 2024.

Observation-minus-background (O–B) values for the clear-sky FY-4B AGRI channel-9 in the CNOP area with 120-km (DAEXP_inCNOP120) and 30-km (DAEXP_inCNOP30) thinning boxes, respectively. It shows that the assimilated data are mainly concentrated in the clear-sky regions over the ocean. Besides, more AGRI observations can be assimilated in DAEXP_inCNOP30 with relatively small O–B values. Fig. 4e presents the track errors of experiments DAEXP_all, DAEXP_inCNOP120, and DAEXP_inCNOP30 for Typhoon Yagi with the initial time at 0000 UTC 3 September 2024. Regarding the track errors for Typhoon Yagi, DAEXP_inCNOP120 shows overall smaller errors compared to DAEXP_all, with particularly significant improvements in the 48-hour track forecast. Furthermore, the enhanced assimilation experiment DAEXP_inCNOP30 shows further improvements in track errors compared to DAEXP_inCNOP120, not only reducing errors in the 0-48 hours but also further reducing track errors after 72 hours. This suggests that by reducing the CNOP-type initial errors optimized for 48 hours, positive effects on later forecasts are also achieved.

4 Conclusions and discussion

In this study, the hybrid FuXi-SHTM model demonstrates significant improvements over the standalone SHTM model, particularly in typhoon track forecasts and precipitation prediction. For Typhoon Yagi (2024), FuXi-SHTM not only provides a more accurate track, aligning closely with observations, but also maintains a more consistent intensity forecast beyond 72 hours. Similarly, for Typhoon Krathon (2024), FuXi-SHTM offers a more reliable typhoon track and intensity forecast compared to SHTM. The inclusion of FuXi's large-scale forecast fields plays a critical role in enhancing the model's performance, particularly in extreme precipitation predictions. Furthermore, the application of the CNOP technique for target observation-assimilation-forecasting optimizes the initial conditions, significantly improving the forecast accuracy, particularly in track predictions for Typhoon Yagi. The assimilation of FY-4B AGRI observations within the CNOP-sensitive area further enhances the model's forecast skill, providing valuable insights into the role of targeted observation in improving typhoon track forecasting.

The potential for further improvement of the FuXi-SHTM hybrid model can be summarized in three key areas. First, the development and enhancement of the FuXi model itself, such as FuXi-ENS, which have improved the forecasting performance of the FuXi model (Zhong et al., 2024). Second, improvements in traditional physical models, such as the further development of convection parameterization schemes and boundary layer parameterization schemes. Future advancements in physical models are critical not only for improving the hybrid model but also for enhancing the performance of ML models. The third and most crucial area is the improvement of the initial fields. Both FuXi and SHTM rely on high-precision analysis fields, and current mainstream analysis fields, such as the ECMWF HRES analysis, are generated using advanced assimilation systems that integrate a large volume of high-quality observations. For example, in this study, satellite data are assimilated in the sensitive area identified by CNOP, which further improves the typhoon track forecasts.

While the competition between traditional NWP models and ML models continues, our focus should not be solely on replacing NWP models using ML models. Instead, efforts should be directed toward the continued refinement of NWP models, including improvements in physical parameterizations and data assimilation processes (Bauer et al., 2015), to enhance our understanding of atmospheric dynamics rather than bypassing fundamental challenges. At the same time, leveraging the complementary strengths of ML and NWP models has proven effective, as the ML-physics hybrid paradigm has already demonstrated its potential to improve forecasts for both large- and small-scale weather systems. As a result, ML-physics hybrid typhoon forecasting models are gradually becoming the mainstream operational paradigm.

Acknowledgments

The final version to be submitted to the journal will include information about other authors. The current version is being handled by the first author.

Open Research

FY-4B AGRI data were collected from the National Satellite Meteorological Center China Meteorological Administration (http://satellite.nsmc.org.cn/portalsite/default.aspx)

References

Bauer, P., Thorpe, A., & Brunet, G. (2015). The quiet revolution of numerical weather prediction. *Nature*, 525(7567), 47–55. https://doi.org/10.1038/nature14956

Ben-Bouallegue, Z., Clare, M. C. A., Magnusson, L., Gascon, E., Maier-Gerber, M., Janousek, M., et al. (2023). The rise of data-driven weather forecasting (arXiv:2307.10128 [physics]). *arXiv*. https://doi.org/10.48550/arXiv.2307.10128

Bi, K., Xie, L., Zhang, H., Chen, X., Gu, X., & Tian, Q. (2023). Accurate medium-range global weather forecasting with 3D neural networks. *Nature*, 619(7970), 533–538. https://doi.org/10.1038/s41586023061853

Bonavita, M. (2024). On some limitations of current machine learning weather prediction models. *Geophysical Research Letters*, 51(12), e2023GL107377. https://doi.org/10.1029/2023GL107377

Budakoti, S., Singh, C., & Pal, P. K. (2019). Assessment of various cumulus parameterization schemes for the simulation of very heavy rainfall event based on optimal ensemble approach. *Atmospheric Research*, 218, 195–206. https://doi.org/10.1016/j.atmosres.2018.12.005

Chen, K., Han, T., Gong, J., Bai, L., Ling, F., Luo, J.-J., et al. (2023). FengWu: Pushing the skillful global medium-range weather forecast beyond 10 days lead (arXiv:2304.02948 [physics]). *arXiv*. https://doi.org/10.48550/arXiv.2304.02948

Ek, M. B., Mitchell, K. E., Lin, Y., Rogers, E., Grunmann, P., Koren, V., et al. (2003). Implementation of Noah land surface model advances in the National Centers for Environmental Prediction operational mesoscale Eta model. *Journal of Geophysical Research: Atmospheres*, 108(D22), 8851. https://doi.org/10.1029/2002JD003296

Hu, X.-M., Klein, P. M., & Xue, M. (2013). Evaluation of the updated YSU planetary boundary layer scheme within WRF for wind resource and air quality assessments. *Journal of Geophysical Research: Atmospheres*, 118, 10,490–10,505. https://doi.org/10.1002/jgrd.50823

Husain, S. Z., Separovic, L., Caron, J. F., Aider, R., Buehner, M., Chamberland, S., ... & Zadra, A. (2024). Leveraging data-driven weather models for improving numerical weather prediction skill through large-scale spectral nudging. *arXiv preprint* arXiv:2407.06100.

Kochkov, D., Yuval, J., Langmore, I., Norgaard, P., Smith, J., Mooers, G., ... & Hoyer, S. (2024). Neural general circulation models for weather and climate. *Nature*, 632(8027), 1060-1066. https://doi.org/10.1038/s41586-024-07744-y

Lam, R., Sanchez-Gonzalez, A., Willson, M., Wirnsberger, P., Fortunato, M., Alet, F., et al. (2023). Learning skillful medium-range global weather forecasting. *Science*, 382(6677), 1416–1421. https://doi.org/10.1126/science.adi2336

Lang, S., Alexe, M., Chantry, M., Dramsch, J., Pinault, F., Raoult, B., Clare, M. C. A., et al. (2024). AIFS-ECMWF's data-driven forecasting system (arXiv:2406.01465 [physics.ao-ph]). *arXiv*. https://doi.org/10.48550/arXiv.2406.01465

Liu, C. C., Hsu, K., Peng, M. S., Chen, D. S., Chang, P. L., Hsiao, L. F., et al. (2024). Evaluation of five global AI models for predicting weather in Eastern Asia and Western Pacific. *npj Climate and Atmospheric Science*, 7(1), 221. https://doi.org/10.1038/s41612024007690

Liu, H. Y., Tan, Z. M., Wang, Y., Tang, J., Satoh, M., Lei, L., ... & Chen, Q. Z. (2024). A hybrid machine learning/physics-based modeling framework for 2-week extended prediction of tropical cyclones. *Journal of Geophysical Research: Machine Learning and Computation*, 1(3), e2024JH000207. `https://doi.org/10.1029/2024JH000207`

Mu, M., Duan, W. S., & Wang, B. (2003). Conditional nonlinear optimal perturbation and its applications. *Nonlinear Processes in Geophysics*, 10(6), 493-501. `https://doi.org/10.5194/npg-10-493-2003`

Mlawer, E. J., Taubmann, S. J., Brown, P. D., Iacono, M. J., & Clough, S. A. (1997). Radiative transfer for inhomogeneous atmospheres: RRTM, a validated correlated-k model for the longwave. *Journal of Geophysical Research*, 102(D14), 16,663–16,682. `https://doi.org/10.1029/97JD00237`

Niu, Z., Zhang, L., Yang, Y., Han, Y., Li, H., Wang, D., ... & Weng, F. (2024). Assimilating FY-4B AGRI Three Water Vapor Channels in Operational Shanghai Typhoon Model (SHTM) Using GSI-based 3DVar Approach. *IEEE Journal of Selected Topics in Applied Earth Observations and Remote Sensing*. `https://doi.org/10.1109/JSTARS.2024.3522056`

Niu, Z., Huang, W., Zhang, L., Deng, L., Wang, H., Yang, Y., ... & Li, H. (2025). Improving typhoon predictions by integrating data-driven machine learning model with physics model based on the spectral nudging and data assimilation. *Earth and Space Science*, 12(2), e2024EA003952. `https://doi.org/10.1029/2024EA003952`

Olivetti, L., & Messori, G. (2024). Do data-driven models beat numerical models in forecasting weather extremes? A comparison of IFS HRES, Pangu-Weather and GraphCast. *EGUsphere*, 2024, 1-35. `https://doi.org/10.5194/egusphere-2024-1042`

Omrani, H., Drobinski, P., & Dubos, T. (2012). Spectral nudging in regional climate modelling: how strongly should we nudge. *Q. J. Roy. Met. Soc.*, 138, 1808–1813. `https://doi.org/10.1002/qj.1894`

Subich, C., Husain, S. Z., Separovic, L., & Yang, J. (2025). Fixing the Double Penalty in Data-Driven Weather Forecasting Through a Modified Spherical Harmonic Loss Function. *arXiv preprint* arXiv:2501.19374.

Thompson, G., Rasmussen, R. M., & Manning, K. (2004). Explicit forecasts of winter precipitation using an improved bulk microphysics scheme. Part I: Description and sensitivity analysis. *Monthly Weather Review*, 132, 519–542. `https://doi.org/10.1175/1520-0493(2004)1322.0.CO;2`

Sun, Y. Q., Hassanzadeh, P., Zand, M., Chattopadhyay, A., Weare, J., & Abbot, D. S. (2024). Can AI weather models predict out-of-distribution gray swan tropical cyclones?. *arXiv preprint* arXiv:2410.14932.

Wang, H., Mu, M., & Huang, X. Y. (2011). Application of conditional non-linear optimal perturbations to tropical cyclone adaptive observation using the Weather Research Forecasting (WRF) model. *Tellus A: Dynamic Meteorology and Oceanography*, 63(5), 939-957. `https://doi.org/10.1111/j.1600-0870.2011.00536.x`

Xu, H., Zhao, Y., Zhao, D., Duan, Y., & Xu, X. (2024). Improvement of disastrous extreme precipitation forecasting in North China by Pangu-weather AI-driven regional WRF model. *Environmental Research Letters*, 19(5). `https://doi.org/10.1088/1748-9326/ad41f0`

Xu, H., Zhao, Y., Dajun, Z., Duan, Y., & Xu, X. (2025). Exploring the typhoon intensity forecasting through integrating AI weather forecasting with regional numerical weather model. *npj Climate and Atmospheric Science*, 8(1), 38. `https://doi.org/10.1038/s41612-025-00926-z`

Zhang, Y., Long, M., Chen, K., Xing, L., Jin, R., Jordan, M. I., & Wang, J. (2023). Skilful nowcasting of extreme precipitation with NowcastNet. *Nature*, 619(7970), 526-532. `https://doi.org/10.1038/s41586-023-06184-4`

Zhong, X., Chen, L., Li, H., Liu, J., Fan, X., Feng, J., ... & Lu, B. (2024). FuXi-ENS: A machine learning model for medium-range ensemble weather forecasting. *arXiv preprint* arXiv:2405.05925.